# MEMS Bimorph Fiber-Gripping Actuators

Mohammad S. Islam
Electrical and Computer Engineering
University of Louisville
Louisville, USA
shafquatul.islam@louisville.edu

Sruthi Sarani Vankayala Computer Science Engineering Gayatri Vidya Parishad Visakhapatnam, India sruthisarani93@gmail.com Sushmita Challa
Electrical and Computer Engineering
University of Louisville
Louisville, USA
sushmita.challa@louisville.edu

Jasmin Beharic
Micro/Nano Technology Center
University of Louisville
Louisville, USA
jasmin.beharic@louisville.edu

Muhemmad H. Yassin
Materials Science & Engineering
University of Illinois at UrbanaChampaign
Urbana, USA
myassin3@illinois.edu

C. K. Harnett
Electrical and Computer Engineering
University of Louisville
Louisville, USA
c0harn01@louisville.edu

Abstract— We investigate mechanical tangling for adhesion of microelectromechanical systems (MEMS) to unconventional carrier materials in the assembly of stretchable electronics. Adhesion plays a crucial role in fabrication, but is a difficult task to realize even on continuous thin films of soft materials like silicone and polyimide. Adhesion becomes more challenging on discontinuous surfaces like fabric meshes, vet these substrates expand the MEMS universe to new materials, and provide new affordances like passage of electronic contacts from one side of a mesh to the other. Microgripper arrays are realized by using conventional micromachining techniques involving optical lithography and etching processes. This paper describes a process that wraps a MEMS gripper around a conductive fiber and reverses the process using electric current to open the gripper. The gripper's electrical resistance serves as a selftemperature sensor over the 20-500 °C range. The fabrication of these mechanical strain-engineered microgrippers are based on metal-oxide bilayer design and carried out using standard microfabrication steps. Beyond their potential for adhering MEMS to fabrics and to flexible/stretchable substrates that are incompatible with or resistant to adhesives, these microgrippers illustrate how MEMS-based microrobots might interact with small-scale (< 200 micron diameter) fibers in manipulation and locomotion activities.

Keywords—MEMS, microgripper, strained bimorphs, microfabrication.

#### I. Introduction

Functional integration of heterogeneous materials can enable novel MEMS design formats to be implemented on substrates with characteristics such as stretchability, breathability, etc. The reversible geometric transformation of MEMS realized through thermal actuation via pulsed current can allow this integration to be real-time configurable.

MEMS actuation can enable scheduled release of environmental samples from microcontainers for analysis [1], while other MEMS based mechanical devices detect fluid flow events [2], steer and modulate light, produce three dimensional electric fields in microfluidics and other applications, and serve as electromagnetic resonators, antenna elements and probes for observing surface topology in atomic force microscopy [3].

Understanding the electrical and mechanical characterization of MEMS microgripper actuation can enable dynamic formatting of functional gripper contacts with fiber substrates. Decision parameters such as electrical contact area, mechanical clasp strength, and latching-

unlatching with the fiber can be controlled by electrical switching between the various stable states of gripper actuation. These actuating MEMS fiber grippers can have a wide scope of applications in microbot technology as fiber crawlers carrying payloads [4]. Contemplating locomotion, micro assembly and micromanipulations on fiber systems helps envision biological vessel networks for microsurgery [5], textile circuit routing [6], and tissue engineering [7].

Various methods realizing MEMS actuation have been demonstrated in literature such as, actuation triggered by light [8], fluid flow, electrothermal actuation [1], [2], electrostatic actuation [9], electromagnetic actuation [10] and piezoelectric actuation [11]. The electro-thermal actuators can be further classified based on the basis of in-plane and out-of-plane actuation. While U-beam/hot-and-cold-arm actuators [12] and V-beam/chevron actuators [13] are employed for horizontal/lateral actuation, the bimorph actuators in this work and others [14] are used for out-of-plane actuation.

MEMS actuators can be bilayer, trilayer [15] or multimorph structures implemented with materials with differential expansion. MEMS researchers have demonstrated bilayers of metal/diamond like carbon or metal/oxide, and trimorphs of metal/polymer/oxide for applications in medicine [16]. Bimorphs of Al/SiO<sub>2</sub> [17], and Cu/W [18] have been used to implement micro-mirrors.

In this work we characterize the fiber gripper actuator response in terms of resistance, temperature, and radius of curvature of the device with respect to current applied at the contact pads. We envision the gripper clasping and detaching from the fiber, and put forth insights of the gripper actuator carrying payloads.

# II. MATERIALS AND METHODS

#### A. Theory and Equations

The MEMS gripper is designed to have 12 gripper arms of length 740  $\mu m$  built in a continuous trace format (Fig. 1) where one of the arms is fixed and connected to contact pads. The gripper's arm trace width is 10  $\mu m$  and its contact pads dimensions are 200  $\mu m$  \* 200  $\mu m$  for the purpose of electrical probing for driving current and enabling thermal actuation. A donut-shaped etch window of 1850  $\mu m$  outer diameter and

inner diameter 330 µm encompassing the gripper is designed such that the gripper center is fixed to the substrate (Fig. 2).

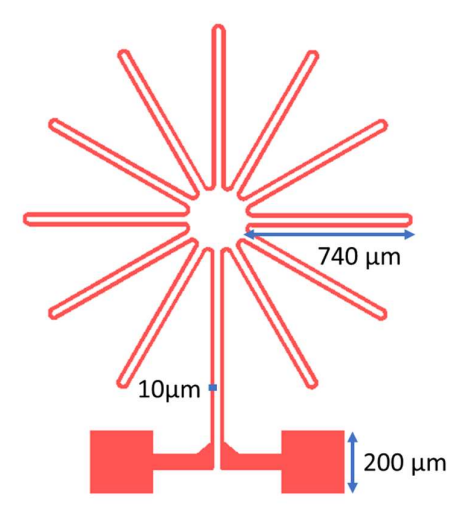


Fig. 1. Bimorph Microgripper Design.

The bimorph microgripper curls to a radius of curvature  $\rho$  when released from the surface due to differential thermal expansion of the bilayers. This is the radius that a working gripper gets to when no current is applied. The curvature, or inverse radius  $1/\rho$ , is given by equation 1:

$$\frac{1}{\rho} = \frac{6\varepsilon(1+m)^2}{d[3(1+m)^2 + (1+mn)\{m^2 + (mn)^{-1}\}]}$$
 (1)

$$\frac{1}{\rho} = \frac{6(d_B - d_A)(t - t_0)(1 + m)^2}{d[3(1 + m)^2 + (1 + mn)\{m^2 + (mn)^{-1}\}]}$$
(2)

where  $\varepsilon$  is the strain mismatch or fractional difference in the unconstrained relaxed lengths of the two layers  $(l_B - l_A)/l_o$ , n is the ratio of the elastic modulus E of the layers,  $(n = E_A/E_B)$  and m is the ratio of their thicknesses d,  $(m = d_A/d_B)$ . Subscripts 'A' & 'B' refer to the upper metal and lower oxide layers, respectively. Eq. 1 could also be represented as Eq. 2 where  $t_o$  is the initial temperature of the gripper, t is the temperature at which the gripper starts to actuate. This equation is useful to get the theoretical radius of curvature of the gripper actuation for a given thermal condition (applied current).

The strain mismatch  $\varepsilon$  is induced by thermal expansion during fabrication, causing the layers to curl up from the substrate at room temperature. When the structure is heated, it opens and flattens, because the top metal layer has a more than 50 times greater thermal coefficient of expansion (TCE) than the oxide layer.  $T_f$  describes the "flat temperature" at which the released pop-up MEMS will become planar again:

$$T_f \approx T_o + \frac{\Delta T_{ox}(\alpha_{si} - \alpha_{ox}) - \Delta T_m(\alpha_{si} - \alpha_m)}{(\alpha_m - \alpha_{ox})}$$
(3)

where (in standard SI units)  $T_o$  is liftoff temperature (room temperature),  $\Delta T_{ox}$  is oxide deposition temperature - liftoff temperature,  $\Delta T_m$  is metal deposition temperature - liftoff temperature,  $\alpha_{Si}$  is silicon TCE,  $\alpha_{ox}$  is oxide TCE, and  $\alpha_m$  is

metal TCE. With increasing current through the metal layer, gripper temperature increases linearly (Fig. 4b).

# B. Gripper Fabrication

The bimorph actuator is fabricated on the Si substrate by depositing strain mismatched layers of different thermal expansion coefficients. A 450 nm thick SiO<sub>2</sub> coating is thermally grown on a silicon wafer by wet oxidation at 1000°C. The oxidized wafer is coated with Shipley 1813 photoresist, and the wafer is exposed on a contact aligner (Karl Suss) to ultraviolet (UV) light through a bright field mask. Image reversal using a Yes oven is carried out followed by flood exposure at the aligner and a development step in MF319 developer. The image reversal process makes the photoresist sidewalls slanted assisting in small features clearing in the lift off process. A Ti-Au metal layer of 480 nm combined thickness (where Ti and Au are 10 and 470 nm, respectively) is deposited on the wafer using a sputtering machine (Lesker PVD75). A lift-off process is carried out in acetone to obtain the metal patterned oxidized wafer. A second photolithography patterning is carried out using a dark field mask containing the torus shaped etch window design. Plasma assisted selective oxide removal is done in a reactive ion etch chamber (March) for about 10 min with 300 mTorr pressure of CF<sub>4</sub>:H<sub>2</sub> at a partial pressure ratio of 50:3 and a RF power of 300 W. The processed wafer is then diced, and each die is wire bonded to a printed circuit board as shown in Fig. 3. A single tinned Cu wire (Karl Grimm) is aligned to the gripper with a tolerance of 400 microns. An isotropic XeF<sub>2</sub> assisted Si etch is carried out using Xactix to release the MEMS gripper arms from the substrate, keeping the center of the device and contact pads attached to the wafer. The overall microgripper fabrication process flow is illustrated in Fig. 2.

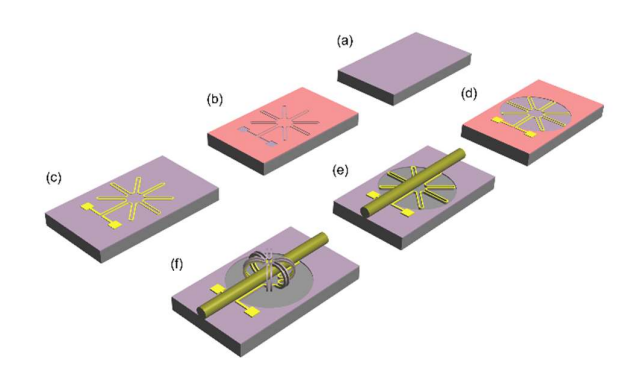


Fig. 2. Microgripper Fabrication Process Flow: (a) 450 nm  $SiO_2$  deposited on Si wafer; (b) Photoresist patterning carried out using Yes oven with gripper design mask; (c) 470 nm Au-Ti sputtering and lift off using acetone; (d) Photoresist patterning for selective etch windows; (e)  $SiO_2$  plasma etch and fiber-tinned Cu alignment; (f) Dry silicon etch to release bimorph actuator arms from the substrate.

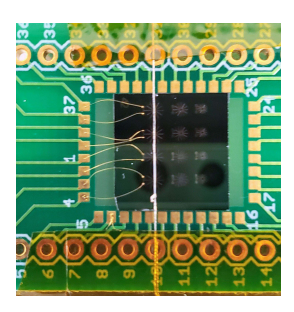
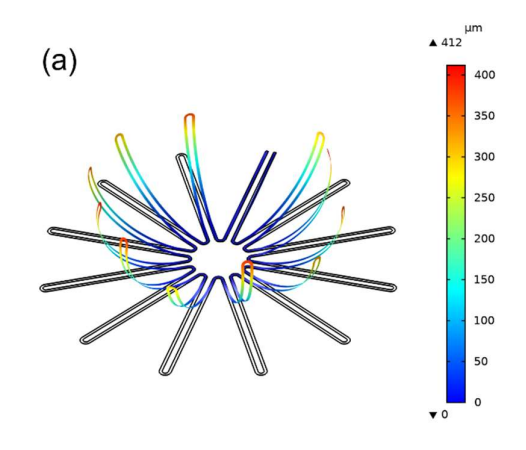


Fig. 3. Fabricated device wire bonded to a printed circuit board.

#### C. Finite Element Analysis

A finite element modeling (FEM) simulation was carried out using COMSOL Multiphysics 5.5 software to analyze the mechanical deformation behaviors of the Au/SiO<sub>2</sub> microgripper due to applied voltage. The microgripper was modeled in accordance with the design dimensions discussed earlier and using original material properties provided in COMSOL material library. Following the construction of the model geometry, material properties are added to the bilayer structure with the top layer chosen as Au, while the bottom layer is assigned to SiO<sub>2</sub>.



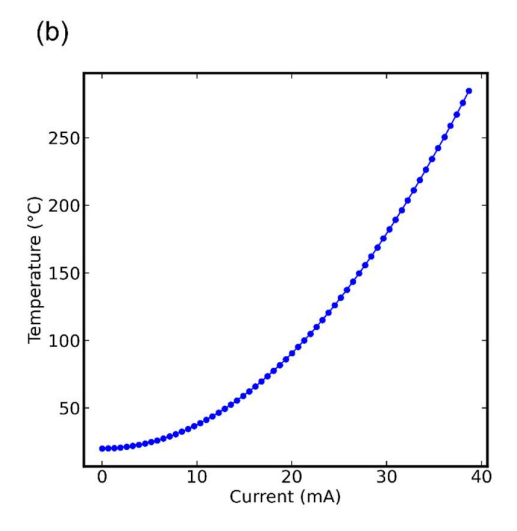


Fig. 4. FEM simulation of the microgripper: (a) deformation with temperature-dependent electrical conductivity; (b) Temperature of the microgripper top layer (Au) for different values of applied current.

For each microgripper arm the anchored surfaces around the center of the microgripper for both Au and SiO<sub>2</sub> layers were assigned to have mechanically fixed surface boundary conditions while other surfaces were kept free to move in the Structural Mechanics module. The finite element simulations were performed using physics-controlled meshing elements with a linear solver. Electric potential ranging from 0-1.5 V is applied on the fixed arm of the microgripper which is connected to the contact pads as presented in Fig. 1. This applied voltage induces an electric current and due to the material's resistivity, in this case Au, the current heats up the structure. The thermally induced stress loads the material and deforms the microgripper arms.

By using the Joule Heating and Thermal Expansion predefined multiphysics interface, COMSOL automatically adds the equations for three physics including the necessary multiphysics couplings. COMSOL modules, Heat Transfer and Structural Mechanics, work in conjunction to model the mechanical deformation and performance of the microgripper structure as a function of temperature which is dependent on the voltage applied. Fig 4(a) illustrates a maximum gripper tip displacement of 412 µm resulting from an applied voltage of 1.5 V. The numerical results of the simulated temperature as a function of applied current are presented in Fig. 4(b).

#### III. RESULTS

# A. Gripper Actuation Results

The device behavior can be analyzed using the following results on gripper resistance, actuation current threshold, current handling capacity, electrical and mechanical insights on thermal actuation.

We tested 34 grippers (1,000  $\mu m$  diameter probing design gripper) for their average resistance when carrying 10 mA of current, the median value was 96  $\Omega$  +/- 31  $\Omega$ , within uncertainty of the theoretical value of 108  $\Omega$ . After testing 16 grippers (1,000  $\mu m$  diameter probing design gripper) for their maximum current density, the median value was 40 mA: vastly superior to the theoretical value of 9.4 mA.

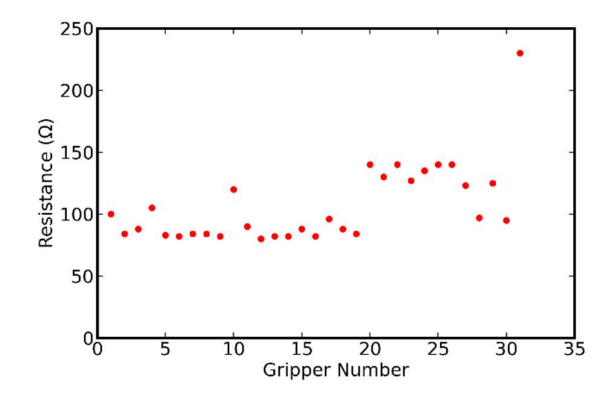


Fig. 5. Scatter plot of the measured resistance across different gripper devices at an applied current of  $10\ mA$ .

Although theoretical, the best temperature approximation where the metal and oxide flatten after release (Eq. 2) is

337°C (based on a metal deposition temperature of 200°C). A model extrapolating the flat temperature vs metal deposition temperature (both above and below 200°C) shows a linear trend.

Pop-up MEMS begin to 'unfold' perceptibly at approximately 6.5 mA. Grippers can handle 1 mA of current for 8.5 minutes uninterrupted. Fig. 6 shows the thermal actuation of the fiber gripper at various levels of applied current.

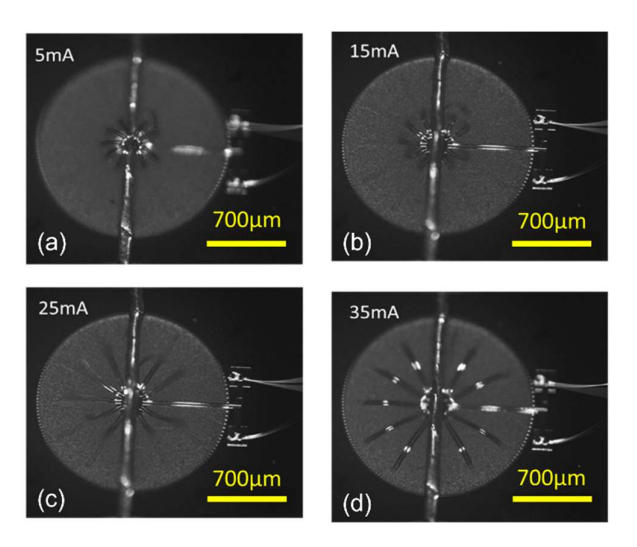


Fig. 6. Current loaded microgripper thermal actuation: (a) Gripper at 5mA applied current; (b) Gripper unfolding at 15 mA; (c) Gripper unfolding at 25 mA; (d) Gripper at 35mA.

### B. Current versus Radius of Curvature

The radius of curvature (ROC) of the top view gripper images at varying currents is obtained through a MATLAB binary and grayscale image analysis algorithm which detects data points on the outer circumference of the gripper. For all the grippers images at different currents (with gripper arms making  $>90^\circ$  and  $<90^\circ$  turns), we applied conditions for detecting outer circumference points at angles where gripper arms were drawn. These data points were averaged to find the mean radius.

We noted that sending greater than 40-50 mA would cause the gripper to permanently open circuit (Table I), and at this point the gripper arms curled more than the theoretical value of radius of curvature of a working gripper. The MEMS microhotplate literature has shown that thermal stresses in current-carrying thin metal films can damage SiO<sub>2</sub> underlayers [19]; a similar mechanism is likely at work here.

For 25 mA, from the gripper image, we can see that the gripper arms have made less than a 90° arc, meaning one cannot read the radius of curvature directly from the top-view image. Therefore, we used python *fsolve* function with input data: top view length and arc-length of the gripper arm for finding the gripper turn angle . Using  $r = L/\theta$ , where L = 740 µm, the radius of curvature was deduced. Fig. 7 shows the change in radius of curvature of the microgripper with respect to applied current. The blue plot shows the theoretical plot of applied current versus gripper radius of curvature derived

TABLE I. GRIPPER RADIUS OF CURVATURE FOR DIFFERENT CURRENTS

Gripper Angle turn and Current Applied	Gripper Image	Description	
> 90° and 0 mA	100 <u>u</u> m	Gripper's original length is 740 µm. After release, the gripper has curled to a radius of curvature (ROC) of 146 µm from the top view for gripper arms at the angles 60-240° from the fixed gripper arm.	
> 90° and 15 mA		Gripper's original length is 740 µm. After release, the gripper has curled to ROC of 250 µm from the top view.	
> 90° and Juiced Out	200µm	Gripper's original length is 740 μm. Once released, the gripper has curled to a ROC of 97 μm from the top view for gripper arms at the angles 30-210° from the fixed gripper arm.	
< 90° and 25 mA	740 μm	Gripper's original length is 740 µm. After release, the gripper has curled to 466 µm from the top view. The ROC after curling was 567 µm (74.8° angle turn).	

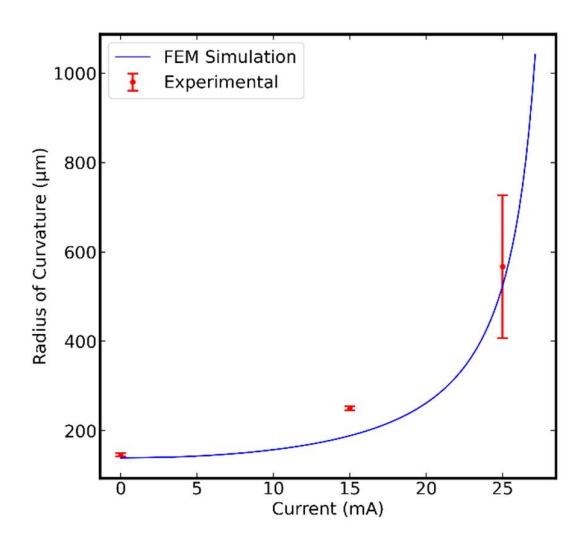


Fig. 7. Blue curve: Theoretical plot of applied current versus gripper radius of curvature derived from Eq. (2) and FEM model in Fig. 4b; Red points: Experimental data of radius of curvature at a given current obtained from image processing on gripper images from Fig. 6.

from gripper radius versus temperature calculation from Eq. (2) and linear interpolation of the temperature values on the

FEM model in Fig. 4(b) to obtain the corresponding current values. Also, the red plot shows the experimental data of radius of curvature along with standard deviation error bars at a given current obtained using image processing algorithm discussed above.

# C. Resistance versus Temperature

Since the resistivity of most metals depends on temperature, we investigated the MEMS structures' function as resistive temperature sensors. Because radius of curvature depends on temperature, and temperature depends not only on current but on heat sinking by the surrounding environment, such self-temperature sensing will be useful in controlling the gripper's position. The current conductance happens through the upper Au metal layer of the bimorph. The positive temperature coefficient of resistivity of gold, indicates an increase in resistance with respect to increase in temperature due to applied current, which is shown in the theoretical plot of the graph Fig. 8. The resistance is calculated by multiplying the theoretical resistivity by l/a, where l is the total trace length of the gripper actuator, which is 15.8 mm, and a is the cross-sectional area, 5  $\mu$ m<sup>2</sup>. The theoretical resistance and temperature values for gold are presented in Table II.

TABLE II. THEORETICAL RESISTANCE AND TEMPERATURE DATA FOR GOLD

T(°C) Theo.	$\rho(\times 10^{-8}) \atop (1/\Omega)$	R (Ω) Theo.	
20	2.214	69.74	
25	2.255	71.03	
27	2.271	71.54	
127	3.107	97.87	
227	3.97	125.06	
327	4.87	153.41	
427	5.82	183.33	
527	6.81	214.52	
627	7.86	247.59	

On the experimental standpoint, currents in the range of 5-45 mA in steps of 5 mA were applied to the device and subsequent resistance values were noted. From the trendline approximation of the theoretical curve, values for the temperature are obtained by linear interpolation into the curve at the measured resistance values (Table III), and the experimental datapoints are plotted (Fig. 8).

TABLE III. EXPERIMENTAL RESISTANCE AND TEMPERATURE DATA FOR GOLD

I (mA)	R(\O)	$\rho(\times 10^{-8}) $ $(1/\Omega)$	T(°C)
	Exp	$(1/\Omega)$	Exp.
5	84.55	2.69	76.42
10	87.5	2.78	87.62
15	87.8	2.79	88.76
20	93	2.95	108.51
25	99	3.14	131.16
30	110.5	3.51	173.46
35	127	4.03	233.86
40	175	5.56	399.16
45	193	6.13	458.01

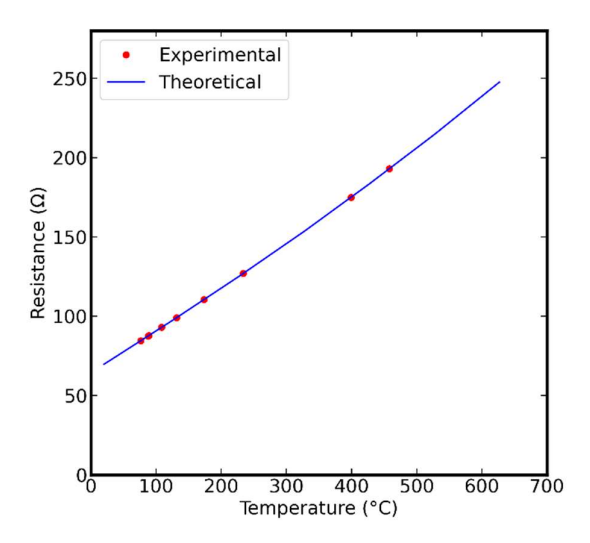


Fig. 8. Blue curve: Theoretical resistance versus temperature for the top metal layer (Au) of the biomorph structure; Red points: Experimental data of measured resistances for 5 to 45 mA applied currents in 5 mA increments, placed on theoretical resistance versus temperature curve.

# D. MEMS gripper latching onto payloads-Fiber, LED

Fig. 9 shows the SEM image of a released microgripper latching onto a fiber. Such a structure might connect a sensor or other device payload to a conductive fiber for power, actuation, or communication. The key to connecting payloads is ensuring payload and fiber compatibility with the MEMS fabrication and release process. The tinned copper wire in Fig. 9, added during fabrication (Fig. 2e), is unaffected by the highly selective XeF2 release process. If applications require optimal contact the gripper radius can be matched to the fiber diameter by working out the theoretical parameters (Eqs. 1 and 2) to get the right radius during fabrication, and fine tuning of the contact area can be done after release by changing the actuation parameters. Other payloads that include silicon, such as logic devices, would need to be passivated with a coating to protect them from the silicon etchant. The CAD model (Fig. 9b) shows how a mini-LED payload (Cree SR1321, 210 x 130 x 110 μm) would connect to a released gripper of similar design.

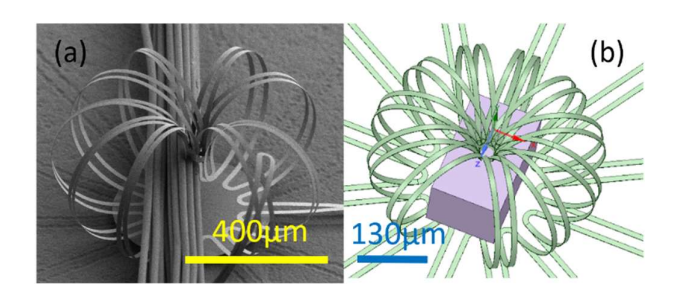


Fig. 9. (a) SEM image of gripper actuator clasping fiber; (b) CAD model of similar gripper design carrying a semiconductor device payload: a mini-LED of dimensions  $210 \ \mu m * 130 \ \mu m * 110 \ \mu m$ .

#### IV. **CONCLUSIONS**

As wonderful as MEMS are, especially when merged with other technologies like ICs and/or photonics on a common substrate, one limitation is that they are made on rigid silicon substrates that do not bend or conform when attached to a soft, flexible, and at times porous substrate. This work investigated a new packaging method that relies on mechanical tangling to integrate MEMS with fibrous materials found in wearables, soft robotics, and other highdeformation applications, and also environments such as filtration systems that require a porous substrate with through-conductance. The reversible clasping demonstrated here could potentially "program" the transfer of devices to fibrous substrates by opening all devices on a wafer and then only closing those to be transferred. Such a selective fan-out approach already makes large-area devices economically from small wafers, as seen in commercial microtransfer printing where large-format displays are made by transferring inorganic LEDs from densely populated donor wafers. Future work on this project will investigate the grippers' pull-off strength and electrical contact resistance, and integrate payloads (Fig. 9) before transfer.

#### ACKNOWLEDGMENT

This project was supported by NSF Award 1849213, "RII Track-1: Kentucky Advanced Manufacturing Partnership for Enhanced Robotics and Structures." We would like to acknowledge Julia Aebersold of the University of Louisville Micro/Nano Technology Center, for expertise on wire bonding devices.

# REFERENCES

- C. K. Harnett, E. V. Moiseeva, B. A. Casper, and L. J. Wilson, "Microscopic containers for sample archiving in environmental and biomedical sensors," in 2010 IEEE Instrumentation Measurement Technology Conference Proceedings, May 2010, pp. 328–331.
- [2] T. M. Lucas, D. A. Porter, J. Beharic, T. A. Berfield, and C. K. Harnett, "Bistability in a symmetric out-of-plane microstructure," Microsyst. Technol., vol. 23, no. 7, pp. 2569–2576, Jul. 2017.
- [3] C. Martin-Olmos, H. I. Rasool, B. H. Weiller, and J. K. Gimzewski, "Graphene MEMS: AFM probe performance improvement," ACS Nano, vol. 7, no. 5, pp. 4164–4170, May 2013. [4] S. Challa, M. S. Islam, and C. K. Harnett, "Fiber-Crawling Microrobots," in 2019 International Conference on Manipulation, Automation and Robotics at Small Scales (MARSS), Jul. 2019, pp. 1–
- [5] A. M. Ghazali, M. N. Hasan, T. Rehman, M. Nafea, M. S. M. Ali, and K. Takahata, "MEMS actuators for biomedical applications: a review," J. Micromech. Microeng., vol. 30, no. 7, p. 073001, May 2020.
- [6] T. Agcayazi, K. Chatterjee, A. Bozkurt, and T. K. Ghosh, "Flexible Interconnects for Electronic Textiles," Adv. Mater. Technol., vol. 3, no. 10, p. 1700277, Oct. 2018.
- [7] S. Wang, Y. Huang, and J. A. Rogers, "Mechanical Designs for Inorganic Stretchable Circuits in Soft Electronics," IEEE Trans. Compon. Packaging Manuf. Technol., vol. 5, no. 9, pp. 1201–1218, Sep. 2015.
- [8] H. Hillmer et al., "Optical MEMS-based micromirror arrays for active light steering in smart windows," Jpn. J. Appl. Phys., vol. 57, no. 852, p. 08PA07, Jul. 2018.
- [9] Y. Zhu and J. Pal, "Erratum: Zhu, Y.; Pal, J. Low-Voltage and High-Reliability RF MEMS Switch with Combined Electrothermal and Electrostatic Actuation. Micromachines 2021, 12, 1237," Micromachines (Basel), vol. 12, no. 11, Nov. 2021, doi: 10.3390/mi12111389.
- [10] [10] X. Lv, W. Wei, X. Mao, Y. Chen, J. Yang, and F. Yang, "A novel MEMS electromagnetic actuator with large displacement," Sens. Actuators A Phys., vol. 221, pp. 22–28, Jan. 2015.
- [11] [11] N. J. Conway, Z. J. Traina, and S.-G. Kim, "A strain amplifying piezoelectric MEMS actuator," J. Micromech. Microeng., vol. 17, no. 4, p. 781, Mar. 2007.
- [12] [12] M. Cauchi, I. Grech, B. Mallia, P. Mollicone, and N. Sammut, "The Effects of Cold Arm Width and Metal Deposition on the Performance of a U-Beam Electrothermal MEMS Microgripper for

- Biomedical Applications," Micromachines (Basel), vol. 10, no. 3, Feb. 2019, doi: 10.3390/mi10030167.
- [13] [13] M. H. Ziko and A. Koel, "Theoretical and Numerical Investigations on a Silicon-based MEMS Chevron type thermal actuator," in 2018 IEEE 18th International Conference on Nanotechnology (IEEE-NANO), Jul. 2018, pp. 1–5.
- [14] [14] S. Algamili et al., "A Review of Actuation and Sensing Mechanisms in MEMS-Based Sensor Devices," Nanoscale Res. Lett., vol. 16, no. 1, p. 16, Jan. 2021.
- [15] [15] M. K. Sonker, "Design and simulation of Tri-morph based MEMS thermal sensor for harsh environment," in 2015 International Conference on Computer, Communication and Control (IC4), Sep. 2015, pp. 1–7.
- [16] T.-B. Xu, J. Su, and Q. Zhang, "Electroactive-polymer-based MEMS for aerospace and medical applications," in Smart Structures and Materials 2003: Smart Electronics, MEMS, BioMEMS, and Nanotechnology, Jul. 2003, vol. 5055, pp. 66–77.
- [17] Q. Chen, H. Zhang, X. Zhang, D. Xu, and H. Xie, "Repeatability study of 2D MEMS mirrors based on S-shaped Al/SiO 2 bimorphs," in The 8th Annual IEEE International Conference on Nano/Micro Engineered and Molecular Systems, 2013, pp. 817–820.
- [18] [18] X. Zhang, B. Li, X. Li, and H. Xie, "A robust, fast electrothermal micromirror with symmetric bimorph actuators made of copper/tungsten," in 2015 Transducers 2015 18th International Conference on Solid-State Sensors, Actuators and Microsystems (TRANSDUCERS), Jun. 2015, pp. 912–915.
- [19] [19] Prasad, Mahanth, and Partha S. Dutta. 2018. "Development of Micro-Hotplate and Its Reliability for Gas Sensing Applications." Applied Physics A: Materials Science & Processing 124 (11): 788.